Accepted Manuscript

Long dwell time orbits for lander-based Mars missions

Emiliano Ortore, Christian Circi, Gian Luigi Somma

PII: S1270-9638(15)00203-5
DOI: http://dx.doi.org/10.1016/j.ast.2015.06.026
Reference: AESCTE 3364

To appear in: *Aerospace Science and Technology*

Received date: 16 August 2014
Revised date: 30 January 2015
Accepted date: 24 June 2015

Please cite this article in press as: E. Ortore et al., Long dwell time orbits for lander-based Mars missions, *Aerosp. Sci. Technol.* (2015), http://dx.doi.org/10.1016/j.ast.2015.06.026

Long dwell time orbits for lander-based Mars missions

Emiliano Ortore*, Christian Circi*, Gian Luigi Somma**

*Department of Astronautical, Electrical and Energetic Engineering, Sapienza University of Rome Via Salaria, 851-881, 00138, Rome, Italy.

Email: emiliano.ortore@uniroma1.it, christian.circi@uniroma1.it

**Faculty of Engineering and the Environment (FEE), University of Southampton, Highfield Campus, Southampton, UK, SO17 1BJ

Email: gl.somma@soton.ac.uk

Abstract

This paper deals with the possibility of retrieving orbits around Mars able to provide long dwell times over a given area of the planet, without needing expensive orbital corrective manoeuvres. After a general description of the fundamental principles associated with the obtainment of the repeating ground track orbits which satisfy the aforesaid requirement, the concepts have been applied to Mars to gain trajectories which make it possible to maximize the daily contact time between a probe orbiting around the planet and a lander on the surface. The lander has been considered as equipped with an antenna of 0.5 m of diameter, working in the bands C, X, Ku, and the cases of both fixed and mobile antenna have been taken into account.

Keywords: Mars exploration; long dwell time; ground track.

1. Introduction

Trajectories around Mars have been investigated and employed to meet a broad range of requirements related to observational constraints (e.g. spatial coverage, resolution, synchronism with the Sun) [1-4], orbital perturbations (e.g. [5]), problems concerning the aerobraking (e.g. [6]) and linked to the release of landers and rovers (e.g. [7]). As for the coverage, the requirement has often been to gain global rather than local coverage, whereas this latter is becoming more and more interesting for Mars exploration. In fact, the feasibility of retrieving trajectories able to provide long dwell times over a given region would translate into both wide intervals of observation of the planet in quasi-steady conditions (useful for both remote sensing and communication applications) and long contact times with a lander (or a rover) positioned inside a certain region of the surface of Mars. Such a requirement may be fulfilled by considering the AreoStationary Orbit (ASO), a circular and equatorial orbit having an altitude of about 17000 km, which (in the Keplerian case) allows the probe to remain permanently steady with respect to the planet [8-9]. However, due to the orbital perturbations, this kind of orbit needs periodic corrective manoeuvres during the entire probe operational life [10-11]. Therefore, in order to avoid the aforesaid corrective manoeuvres and thus extend the probe operational life, it is important to find alternative orbits to the ASO, which are able to guarantee long dwell times over a given region of Mars without requiring orbital corrections associated with expensive velocity variations. In [12], elliptical orbits which make the fulfilment of this goal possible have been obtained. However, in the cited study, the requirement of long dwell time has been considered as a secondary property with respect to the principal one, concerning the design of periodic orbits for monitoring time-varying phenomena. In fact, the argument of pericentre of two particular orbits, already designed to meet requirements based on solar illumination conditions, has been set so as to obtain, in an orbit arc around the apocentre, a behaviour similar to the one offered by the ASO. For such reasons, in the present paper, the feasibility of gaining orbits able to guarantee long dwell times over a given area of Mars has been

investigated. After having described the basic concepts related to obtaining trajectories which provide both cyclic observations and long dwell times (Sect. 2), such concepts have been applied to Mars (Sect. 3), gaining orbits at critical inclination which make the fulfilment of these conditions possible without requiring expensive orbital manoeuvres. Then, the most profitable solutions have been investigated to optimise the lander-probe link time, assuming the constraint of daily contact (Sect. 4).

2. Orbital properties

In a planetary observation mission, a fundamental requirement is the feasibility of observing a given region at regular time intervals and this condition can be fulfilled by considering repeating ground track orbits, also called periodic orbits [13]. In addition to this, another requirement is considered here: the possibility to observe a region with long dwell times. Such a property is achieved if, in a wide time interval, the sub-probe point (intersection between the position vector of the probe and the surface of the planet) is characterized by small shifts with respect to the surface of the planet. These two requirements, strictly related to the probe ground track (Sect. 2.1), will firstly be discussed separately (Sect 2.2 and Sect. 2.3) and then matched (Sect. 3) in order to obtain both repeated and long-lasting observations of Mars.

2.1 Ground track determination

The motion of a probe around a planet can be described in a reference system (X, Y, Z) centred at the centre of mass of the planet and having X axis given by the intersection between equatorial plane of the planet and plane of the orbit of the planet around the Sun, Z axis coincident with the polar axis of the planet (rotation axis of the planet) and Y axis defined so as to form a right reference frame. In this reference, the instantaneous values of the absolute longitude λ and of the

latitude ϕ of the sub-probe point can be expressed as a function of the orbit elements of the probe. According to Fig. 1, the relationships representing this correspondence (coming from spherical trigonometry) can be written as:

$$\lambda(t) = \Omega + \alpha = \Omega + tg^{-1}(tg\xi \cdot \cos i) \qquad (1)$$

$$\phi(t) = \sin^{-1}(\sin i \cdot \sin \xi) \qquad (2)$$

where t is the time, α is the angle (measured on the equatorial plane) between the nodal line and the meridian related to the position of the sub-probe point and Ω, i, ξ are, respectively, the instantaneous values of the Right Ascension of the Ascending Node (RAAN), of the orbit inclination and of the argument of latitude of the probe ($\xi = \omega + \theta$, with $\omega =$ argument of pericentre and $\theta =$ true anomaly of the probe).

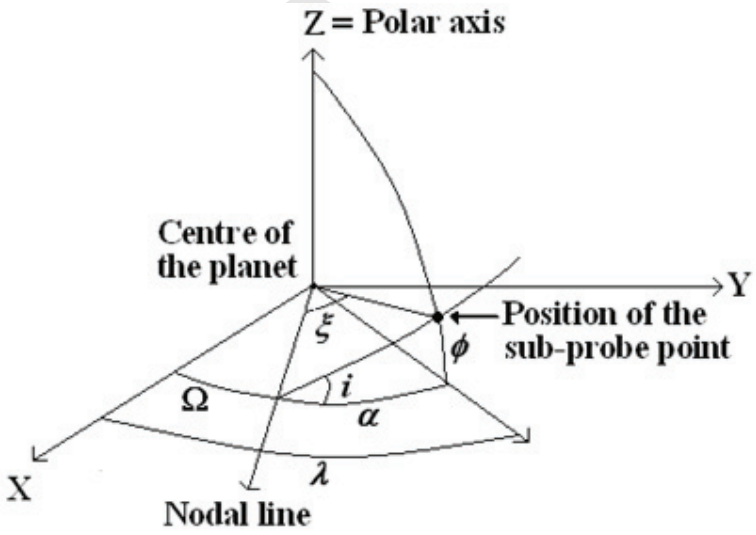

Figure 1. Sub-probe point in the (X, Y, Z) reference frame for a prograde orbit.

Therefore, once the values of Ω, ξ and i are known, it is possible to retrieve λ and ϕ by Eqs. (1) and (2). Of course, in the general case of "perturbed Keplerian motion", it is necessary to take the

temporal variations of the orbit elements into consideration ($\dot{\Omega}$, $\dot{i}$, $\dot{\xi} = \frac{h}{r^2} - \dot{\Omega}\cos i$, with $\mathbf{h} = \mathbf{r} \times \mathbf{v}$ angular momentum per unity of mass of the probe, $\mathbf{r}$ position vector of the probe and $\mathbf{v}$ velocity of the probe), which lead to a continuous modification of the spherical triangle formed by α, ϕ and ξ in Fig. 1. To construct the ground track of a probe, it is necessary to know the temporal trends of the geographical longitude $\lambda_G(t)$ and of the latitude $\phi(t)$. While the latitude is given by Eq. (2), the geographical longitude of the sub-probe point can be retrieved by subtracting, from the absolute longitude λ (Eq. (1)), the reference longitude, which varies as $\omega_P t$, where ω_P is the angular velocity of the planet around its polar axis (in this paper the Airy-0 longitude has been assumed as a reference longitude).

2.2 Periodicity condition

As mentioned, a fundamental requirement is represented by the feasibility of observing a certain zone at regular time intervals. In the present study, the fulfilment of this goal is particularly important because it allows a probe to periodically gain contact with a lander on the surface of the planet. To satisfy this objective, it is possible to design an orbit whose ground tracks repeat themselves after a given time interval (repeating ground track orbit). This condition is satisfied if $mD_n = RT_n$, where D_n is the nodal day of the planet (time elapsing between two consecutive nodal line crossings given by a point on the equator of the planet), m is the integer number of nodal days after which the ground track is repeated (revisit time), T_n is the nodal period of the probe (time elapsing between two consecutive ascending node passes) and R is the integer number of nodal periods accomplished in m nodal days (R and m are prime one to the other). Taking into consideration the zonal harmonic J_2 of the gravitational field (planetary oblateness), it is possible to find an analytical solution for the semi-major axis of a repeating ground track orbit [12]:

$$a^{3.5} + b_1 a^2 + b_2 = 0 \qquad (3)$$

where:

$$b_1 = -\frac{\sqrt{\mu_P}}{q\omega_P},$$

$$b_2 = -\frac{3J_2 R_P{}^2\sqrt{\mu_P}}{2\omega_P(1-e^2)^2}\left\{\frac{1}{2q}\left[\left(5+3\sqrt{1-e^2}\right)\cos^2 i-\sqrt{1-e^2}-1\right]-\cos i\right\},$$

R_P is the mean equatorial radius of the planet, μ_P is the gravitational constant of the planet, e is the orbit eccentricity and the parameter q represents the number of orbits per day (orbits and day are counted with respect to the nodal line: $q = D_n/T_n = R/m$). Assuming a certain value for the orbit inclination, Eq. (3) provides a curve which links semi-major axis and eccentricity, for each value of q. This curve, referred to as curve of periodicity, gives all the repeating ground track orbits corresponding to those i and q values. In particular, the choice of integer values for the parameter q leads to the possibility of revisiting every day the same region of the planet (the same ground tracks are repeated at a regular interval of one nodal day).

2.3 Synchronism condition

The other principal requirement of this study is related to the possibility of obtaining long permanence over a given region of the planet and this requirement can be fulfilled designing orbits whose sub-probe point is quasi-steady with respect to the surface for a long part of the orbital period. With reference to Fig. 2, point P can be considered both as a sub-probe point and as a point belonging to the planet. In the first case, the eastward component of the velocity of the sub-probe point (v_{EP}), which is in a plane parallel to the equatorial plane (projection of $\mathbf{v}$ on the equatorial plane and then in the eastward direction), can be written as:

$$v_{EP} = \omega_Z R_P \cos\phi \qquad (4)$$

where ω_Z is the angular velocity of the probe in the motion of rotation with respect to the polar axis of the planet. In the second case, the velocity of point *P*, considered as in-built to the surface of the planet at a latitude ϕ, is given by:

$$v_P = \omega_P R_P \cos\phi \qquad (5)$$

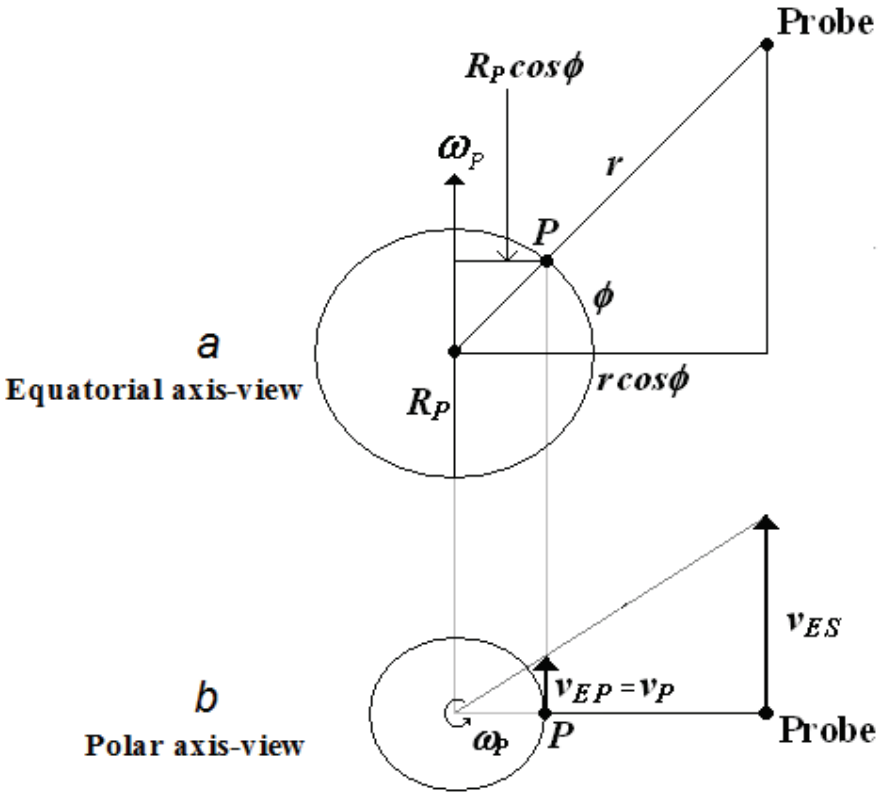

Figure 2. Velocity of the probe in synchronism conditions.

If, at a given instant, the following equality is satisfied (it is possible only if $i < 90$ deg, which also implies $\phi < 90$ deg, according to Eq. (2)):

$$v_{EP} = v_P \qquad (6)$$

then the sub-probe point does not move in either East or West direction and, if $i > 0$, the ground track shows a vertical tangent (the sub-probe point moves from West to East when $v_{EP} > v_P$, while

it moves from East to West when $v_{EP} < v_P$). When this condition is verified, it is $\omega_Z = \omega_P$, which shows how probe and planet constitute an unique rigid body rotating around the polar axis (the sub-probe point has the same motion of rotation as the planet around the polar axis). In general, this state, referred to as synchronism condition, can be achieved only by particular orbits and only for some values of true anomaly. In all the other points the slope of the ground track will depend on the difference between ω_Z and ω_P (or, similarly, between v_{EP} and v_P), related to the orbital elements and to the latitude of the sub-probe point (or, similarly, to the true anomaly of the probe). According to Fig. 2*b*, in synchronism condition, the eastward projection of the probe velocity (v_{ES}) is given by $v_{ES} = \omega_P r \cos\phi$, leading to:

$$\frac{v_{ES}}{r\cos\phi} = \omega_Z = \omega_P \qquad (7)$$

The dependence of ω_Z on the latitude of sub-probe point translates into an influence of ϕ on the ground track shape. As a matter of fact, inclined circular orbits (characterized by a constant velocity equal to $\sqrt{\mu_P / r}$) can achieve the synchronism condition with the planet at high enough latitudes. For example, a circular areosynchronous orbit (which is the analogous of the geosynchronous orbit for Mars) presents two pairs of points, symmetrical with respect to the nodal line of the orbit, in which Eq. (7) is satisfied. The related ground track, characterized by an "eight figure", shows four vertical tangents, two in the ascending and two in the descending part of the orbit. For an elliptical orbit, the synchronism condition (Eq. (7)) can be set at the apocentre of the orbit, taking the following form:

$$\frac{v_A}{r_A\cos\phi_A} = \omega_P \qquad (8)$$

where v_A is v_{ES} computed at the apocentre, $r_A = a(1+e)$ is the radius at the apocentre and ϕ_A is the latitude of the sub-probe point with the probe at the apocentre:

$$\cos\phi_A = \sqrt{1-\sin^2\phi_A} = \sqrt{1-\sin^2 i \sin^2 \xi_A} = \sqrt{1-\sin^2 i \sin^2(\omega+180°)} = \sqrt{1-\sin^2 i \sin^2 \omega} \qquad (9)$$

with ξ_A argument of latitude at the apocentre. Since at the apocentre the projection of the velocity of probe on the equatorial plane is entirely eastward, the velocity v_A can be obtained from its components $v_{A,X}$, $v_{A,Y}$ on the axes X, Y:

$$v_{A,X} = \sqrt{\frac{\mu_P(1-e)}{r_A}}(\cos\Omega\sin\omega + \sin\Omega\cos i\cos\omega) \qquad (10)$$

$$v_{A,Y} = \sqrt{\frac{\mu_P(1-e)}{r_A}}(\sin\Omega\sin\omega - \cos\Omega\cos i\cos\omega) \qquad (11)$$

$$v_A = \sqrt{{v_{A,X}}^2 + {v_{A,Y}}^2} = \sqrt{\frac{\mu_P(1-e)}{r_A}(\sin^2\omega + \cos^2 i\cos^2\omega)} \qquad (12)$$

Thus, introducing Eqs. (9) and (12) in Eq. (8) the synchronism condition at the apocentre can be expressed trough an equation in which the semi-major axis is a function of the orbit eccentricity, of the orbit inclination and of the argument of pericentre:

$$a = \left[\frac{\mu_P}{{\omega_P}^2}\frac{1-e}{(1+e)^3}\frac{\sin^2\omega + \cos^2 i\cos^2\omega}{1-\sin^2 i\sin^2\omega}\right]^{1/3} \qquad (13)$$

The RAAN identifies the longitude of the observed region but it has no influence on the synchronism condition.

3. Application to Mars

In this Section, after a general discussion about the concept of long dwell time orbits characterized by q >1 (Sect. 3.1), q =1 (Sect. 3.2) and q <1 (Sect. 3.3), the two requirements introduced in Sect. 2

(periodicity and synchronism) are merged and applied to the case of Mars so as to gain optimal solutions for this planet (Sect. 3.4), assuming the constraint of daily contact between lander and probe.

3.1 Dwell time orbits with q > 1

In this case, it is possible to design the orbit setting the synchronism condition at the apocentre, according to Eq. (13). However, in this way, at all the other points of the orbit different from the apocentre it is $v_{EP} > v_P$ and this does not lead to a maximization of the dwell time of probe over a given area (case 2 in Fig. 3*a*; the track is progressed according to the direction of the arrow). In fact, to extend the dwell time over a given region, it is necessary to set an eastward component of the velocity of the probe at the apocentre which is smaller than the velocity of synchronism (case 1 in Fig. 3*a*). In such a way, trajectories in which the synchronism condition is satisfied at points of the orbit that are symmetrical with respect to the apocentre are obtained and along an orbital arc around the apocentre the sub-probe point will present small shifts with respect to the planet. This result is achieved by increasing the orbit eccentricity with respect to the case of synchronous apocentre. While in the orbit these synchronous points are symmetrical with respect to the apocentre, due to the dependence on the latitude (Eq. (7)), the sub-probe points corresponding to the synchronism condition (synchronous sub-probe points), apart from the cases $\omega = 0$, $\omega = 180$ deg (synchronous sub-probe points at opposite latitude) and $\omega = 90$ deg, $\omega = 270$ deg (synchronous sub-probe points at the same latitude), are in general not symmetrical with respect to the sub-probe point related to the apocentre (Fig. 3*b*).

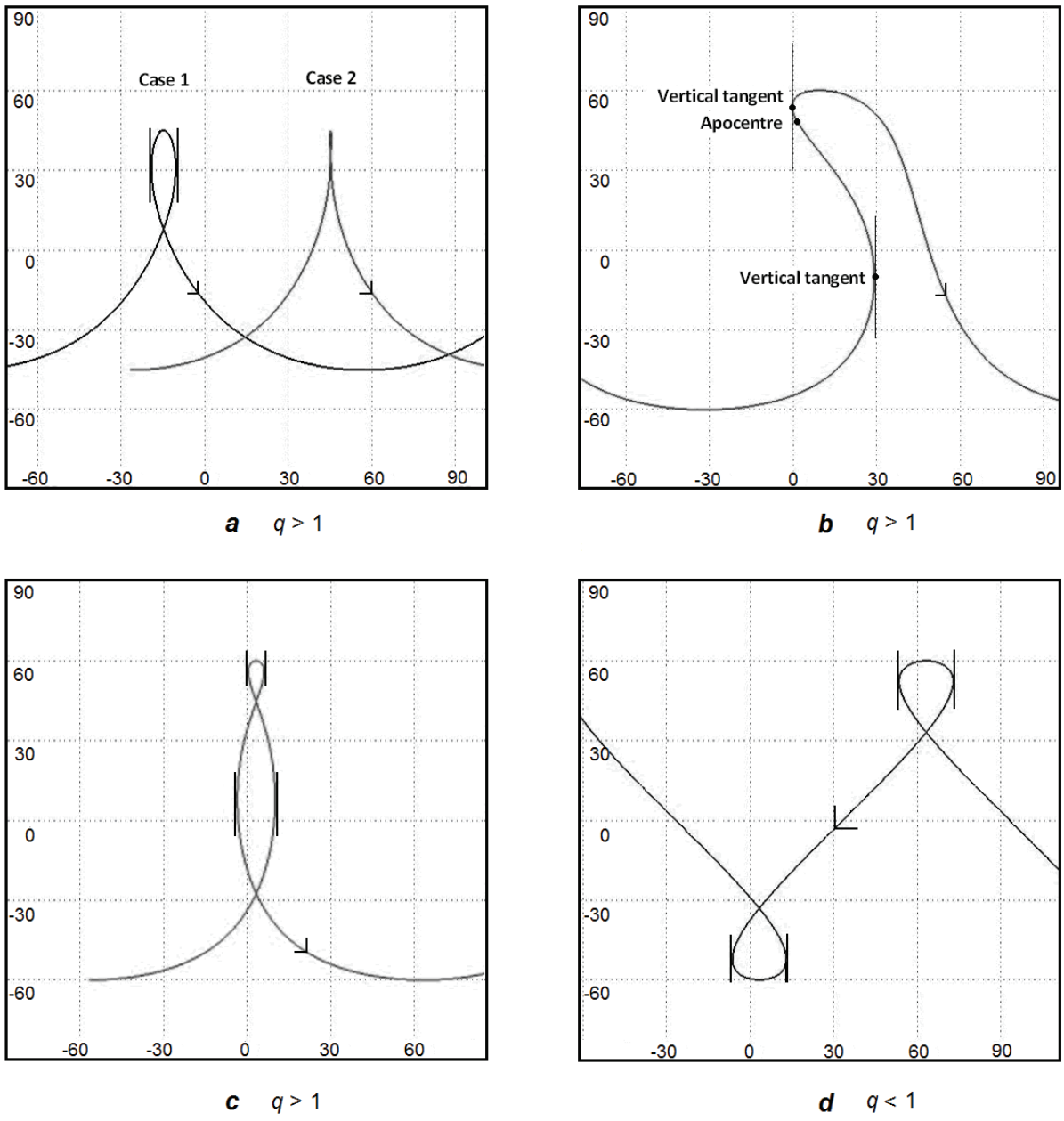

Figure 3. Examples of ground tracks on Mars.

Usually the synchronism condition is verified at two points, but it is also possible to have two pairs of points in which Eq. (7) is satisfied (example in Fig. 3*c*, where the ground track shows the presence of two pairs of vertical tangents). Table 1 reports the orbit elements related to the examples in Fig. 3.

Ground track	*a* [km]	*e*	*i* [deg]	*ω* [deg]	*R/m*
a, case 1	14531.0	0.500	45	270	5/3
a, case 2	14531.0	0.443	45	270	5/3
b	14066.0	0.600	60	240	7/4
c	15588.4	0.500	60	270	3/2
d	24745.1	0.000	60	Not defined	3/4

Table 1. Orbit elements related to the ground tracks of Fig. 3.

3.2 Dwell time orbits with $q = 1$

The value $q = 1$ identifies the category of the areosynchronous orbits. In this case, the orbits allow a dwell time over a fixed region of the planet that is observed at a regular time interval of one nodal day. The ASO represents a particular case of areosynchronous orbit in which the synchronism condition is satisfied at each point of the orbit (the ground track reduces to a point) and the same region of the planet in constantly observed (apart from perturbative effects).

3.3 Dwell time orbits with $q < 1$

As said, the sub-probe point moves from East to West if $v_{EP} > v_P$ ($\omega_Z > \omega_P$) and from West to East if $v_{EP} < v_P$ ($\omega_Z < \omega_P$). In the case $q < 1$, due to the high altitude of the orbits, typically $v_{EP} < v_P$. However, at higher latitudes, according to Eq. (7), the ground track can form loops because of the increase of ω_Z consequent to the decrease of $\cos\phi$ and to the increase of v_{ES} (example in Fig. 3*d*). In general, the formation of these loops may be exploited to obtain long dwell times over the region underlying the loops. However, with $q < 1$ it is not possible to gain a daily revisit time over the same zone ($m = 1$) and, for this reason, this case has not been taken into consideration in the present study. In fact, the constraint that lander and probe can have daily contact has been assumed here.

3.4 Longest daily dwell time orbits

As mentioned, orbits that are both periodic (with $m = 1$) and characterized by long dwell times have to be determined. To this end, the results coming from Eq. (3) have to be matched with the ones coming from Eq. (13). Fig. 4 shows the curves of periodicity for Mars (solutions of Eq. (3)) with i = 63.43 deg and q =1, 2, 3, 4 ($J_2 = 1.955454 \cdot 10^{-3}$, $R_P = 3396.2$ km, $\mu_P = 42828$ km^3/s^2, $\omega_P = 7.08822 \cdot 10^{-5}$ rad/s). Greater values of q have not been considered since, being associated with lower orbital altitudes, they produce lower dwell times over a fixed area. The choice of the critical inclination (63.43 deg) allows the elimination of the perturbative effects related to the planetary oblateness producing the apsidal line motion (Mars is a J_2-predominant planet). Other inclination values have not been taken into consideration because the effects due to Mars's oblateness on the rotation of the apsidal line have proved to be so important as to determine a displacement, in relatively short times, of the Mars' region which is positioned below the orbit arc around the apocentre. On the other hand, the choice $m = 1$ (q integer implies $m = 1$) gives the possibility of revisiting every day the same region of the planet and thus of gaining daily contact with a lander on the surface. The upper limits for the orbit eccentricity have been determined so as to obtain an altitude of pericentre equal to 300 km and thus limiting the drag effects.

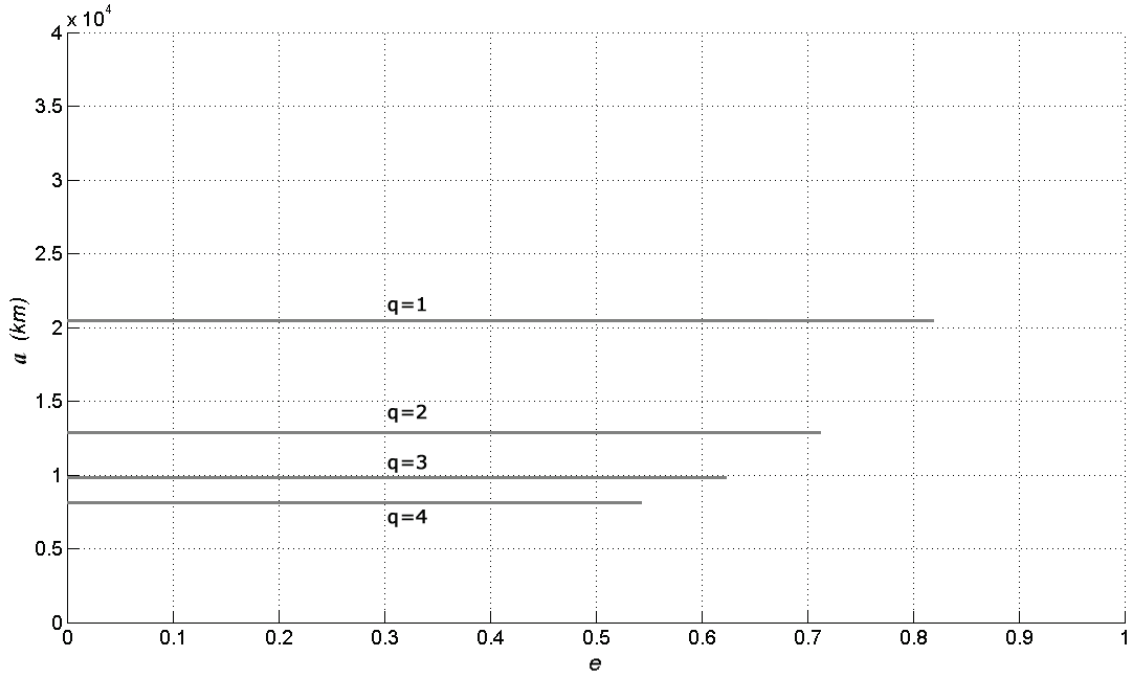

Figure 4. Curves of periodicity around Mars for orbits at critical inclination.

Note that, although the dependence of the semi-major axis on the orbit eccentricity is rather weak (the curves in Fig. 4 seem to be quasi-constant in the scale considered for the semi-major axis), only in the Keplerian case, where the parameter q is simply given by the ratio between sidereal period of the planet (T_P) and Keplerian period of the probe ($q = T_P / (2\pi\sqrt{a^3 / \mu_P})$), the semi-major axis does not depend on the eccentricity. Fig. 5 shows the solutions of Eq. (13), for orbits around Mars characterized by i = 63.43 deg, considering a step of 15 deg for the argument of pericentre. Each point of the curves, identified by a triplet of values (a, e, ω), corresponds to an orbit characterized by an apocentre which is synchronous with Mars. For a fixed value of ω, the semi-major axis decreases for increasing values of the eccentricity.

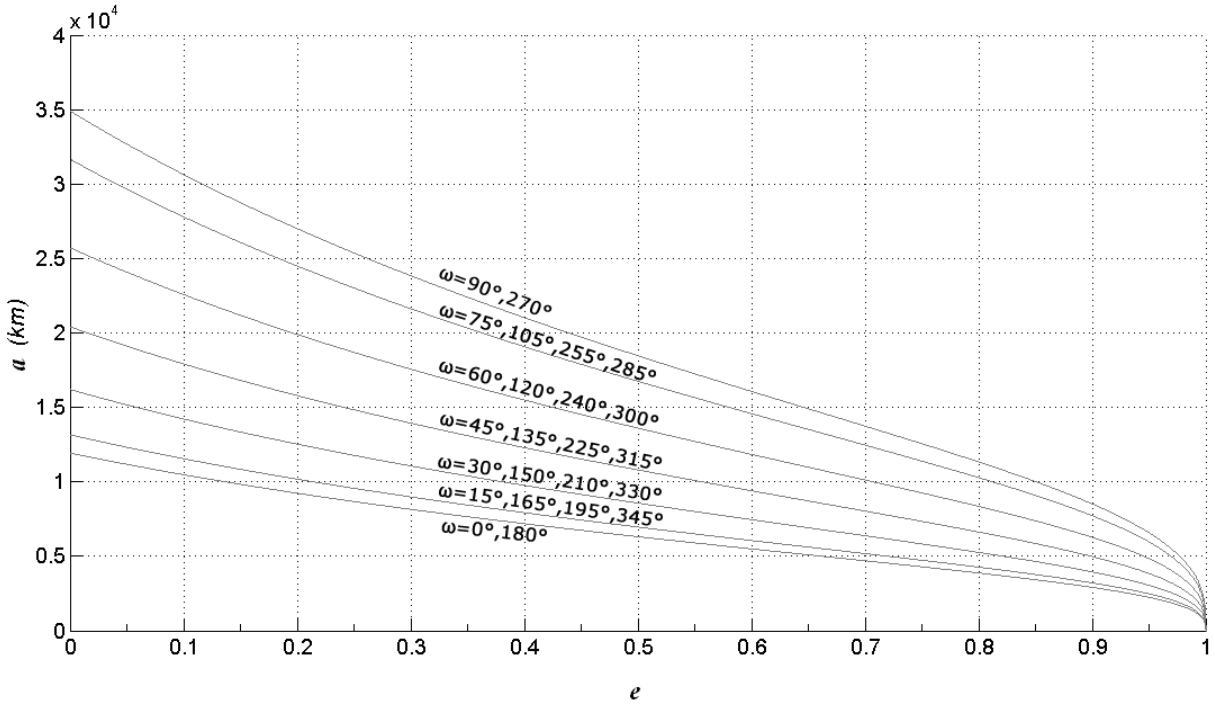

Figure 5. Orbits at critical inclination with synchronous apocentre.

In order to gain solutions that allow cyclic observations of a given target with a revisit time of one nodal day and long dwell times, the results of Fig. 4 have to be merged with the ones of Fig. 5. Thus, Fig. 6 shows the intersection points of the curves of Fig. 4 with the ones of Fig. 5 and Table 2 reports the related orbit elements (with pericentre r_P and apocentre r_A). The solutions A refer to q = 1, the solutions B refer to q = 2, the solutions C to q = 3 and D to q = 4.

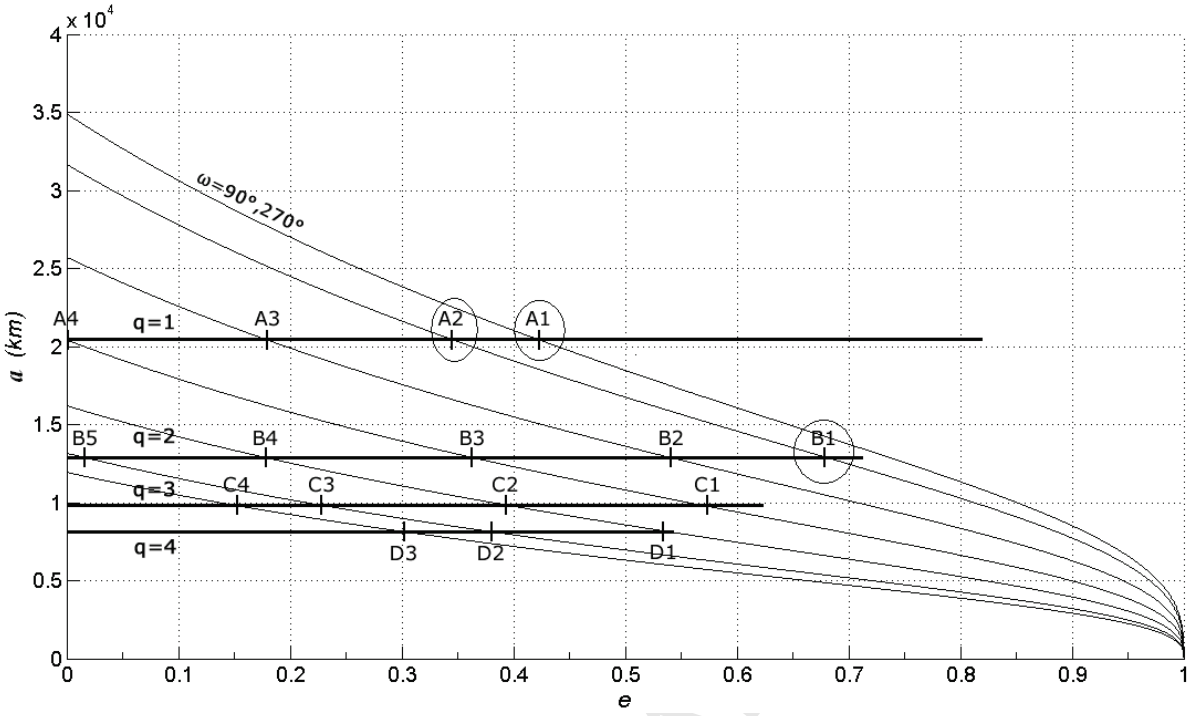

Figure 6. Intersection points of the curves of Figs. 4 and 5.

Solution	a [km]	e	r_A [km]	r_P [km]	ω [deg]
A1	**20426.6**	**0.4233**	**29073.2**	**11780.0**	**270**
A2	**20426.7**	**0.3462**	**27498.4**	**13355.0**	**255**
A3	20426.9	0.1795	24093.5	16760.3	240
A4	20426.9	0.0000	20426.9	20426.9	225
B1	**12862.2**	**0.6818**	**21631.6**	**4092.8**	**255**
B2	12864.9	0.5420	19837.7	5892.1	240
B3	12866.1	0.3648	17559.7	8172.5	225
B4	12866.6	0.1797	15178.7	10554.5	210
B5	12866.7	0.0176	13093.2	12640.2	195
C1	9813.0	0.5706	15412.3	4213.7	225
C2	9815.6	0.3962	13704.5	5926.7	210
C3	9816.6	0.2298	12072.5	7560.7	195
C4	9816.9	0.1520	11309.1	8324.7	180
D1	8095.7	0.5428	12490.0	3701.4	210
D2	8099.1	0.3838	11207.5	4990.7	195
D3	8100.0	0.3059	10577.8	5622.2	180

Table 2. Orbits at critical inclination with synchronous apocentre and daily revisit time.

The solutions reported in Table 2 guarantee different intervals of permanence over a given area and therefore different potential lander-probe contact times. For this reason, a selection of the retrieved solutions, based on such a requirement, has to be carried out. To this end, Fig. 7 shows the daily contact times, in band C (frequency ν = 4 GHz), between a probe positioned over the orbits of Table 2 and a lander located in the sub-probe point corresponding to the apocentre of the orbit. The lander is equipped with a fixed antenna (parabolic reflector) having a diameter of D = 0.5 m and, indicating with G the antenna maximum gain, the angle coverable by the antenna ($\theta_{3\mathrm{dB}}$) corresponds to a gain equal to $G/2$ (reduction of 3 dB with respect to G). More in particular, the following relationships have been used [14]:

$$G = \eta\left(\frac{\pi D}{\lambda}\right)^2 \qquad (14)$$

$$\theta_{3\mathrm{dB}} = 70\frac{\lambda}{D} = \sqrt{\frac{\eta\pi^2(70)^2}{G}} \qquad (15)$$

where η is the efficiency of the antenna aperture (assumed equal to η = 0.6), λ is the signal wavelength ($\lambda = c/\nu$, with c = propagation speed of the electromagnetic radiation in a vacuum) and the number 70 in Eq. (15) represents a proportionality coefficient, expressed in degrees, depending on the antenna geometry and on the efficiency of antenna aperture illumination (the same assumptions have been kept in Sect. 4).

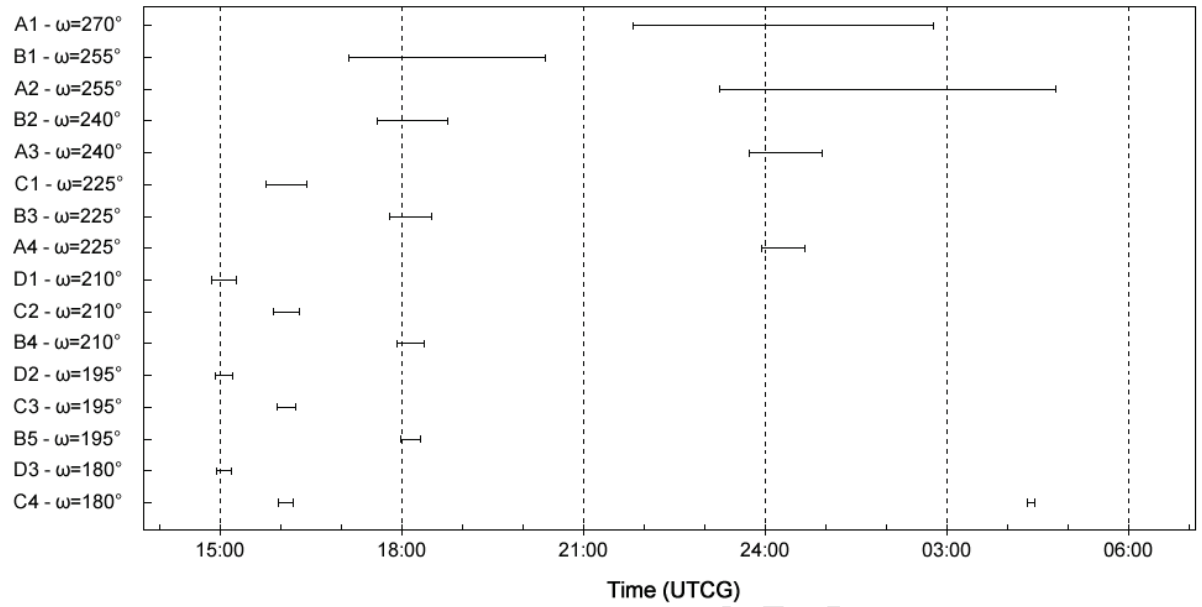

Figure 7. Daily contact time between probe and lander in band C for the orbits of Table 2.

Fig. 7 shows that the longest contact times occur for the first three solutions (A1, B1 and A2). The same conclusions can be achieved considering other communication bands. For this reason, the three aforesaid solutions have been selected and in Sect. 4 they will be investigated in terms of lander-probe contact time.

4. Lander-probe contact time

In this Section, an analysis of the performances of the three selected solutions A1, B1, A2 in terms of contact time between lander and probe has been carried out. This investigation has led to the determination of the conditions, in terms of orbit shape and lander location, able to maximize the daily interval in which, at a given communication frequency, a probe orbiting around the planet remains in contact with a lander. In fact, orbit eccentricity and lander position can be properly adjusted so as to improve the contact times with respect to the ones related to orbits A1, B1 and A2 (Table 2). In particular, given that orbit eccentricity and lander position represent two parameters

that together contribute to the achievement of the optimal solution, the determination of the optimal conditions for these parameters has been carried out taking them into consideration simultaneously. Unlike the value of optimal eccentricity, the optimal lander position depends on the communication frequency.

For solution B1, being $q > 1$, it is possible to extend the lander-probe contact time considering an orbit eccentricity greater than the one related to a synchronous apocentre. For this reason, an analysis aimed at determining the optimal value of e has been executed, considering orbits identified by the periodicity curve $q = 2$ (Fig. 4) and right-shifted with respect to its intersection with the curve of Fig. 5 related to $\omega = 255$ deg (the argument of pericentre of these orbits has to be kept equal to $\omega = 255$ deg). For this solution, the contact time increases as the eccentricity increases and therefore the longest contact time corresponds to the lower limit of the altitude of pericentre (300 km), introduced to limit the drag effects. Thus, the optimal increment is $\Delta e = 0.0294$, which leads to an eccentricity of 0.6818+0.0294 = 0.7112 (solution B1′ in Fig. 8*b*). The corresponding variation of semi-major axis, needed to keep the solution on the curve of periodicity, is equal to 1 km and leads to a semi-major axis of 12862.2 – 1 = 12861.2 km.

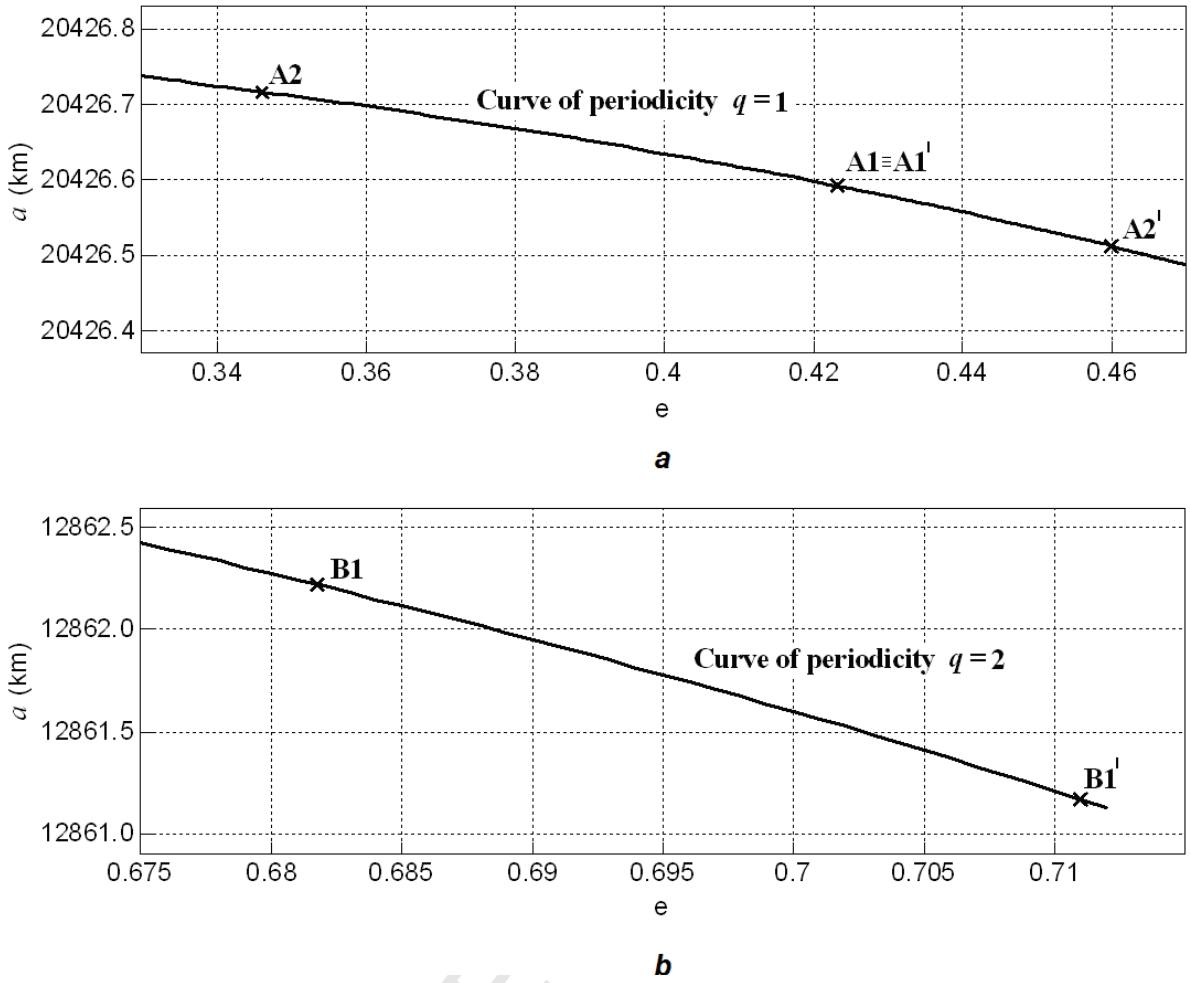

Figure 8. Optimal solutions in terms of orbit shape.

The same analysis has been carried out for the two areosynchronous solutions (Fig 8*a*). For solution A1 no increment of contact time has been obtained as the eccentricity varies with respect to the value in Table 2 and therefore the optimal solution is the one having an apocentre synchronous with Mars (A1′ ≡ A1). For solution A2 the optimal increment of *e* is 0.1135, leading to an eccentricity of 0.3462+0.1135 = 0.4597, which leads a semi-major axis equal to 20426.5 km (solution A2′, corresponding to a reduction of 0.2 km with respect to solution A2). Table 3 summarizes the obtained results.

Solution	a [km]	e	ω [deg]
A1′≡ A1	20426.6	0.4233	270
A2′	20426.5	0.4597	255
B1′	12861.2	0.7112	255

Table 3. Optimal orbit shape.

Figs. 9*a*, 10*a* and 11*a* show the ground tracks of the solutions optimized in terms of orbit shape so as to gain the maximum lander-probe contact time (solutions A1, B1′, A2′). Figs. 9*b*, 10*b* and 11*b* represent zooms of the rectangular areas highlighted in Figs. 9*a*, 10*a* and 11*a*. These figures show the optimal lander positions in the bands C (ν = 4 GHz), X (ν = 8 GHz) and Ku (ν = 12 GHz), along with the related circles delimiting the link areas between lander and probe in the aforesaid bands. The plotted circles refer to the worst conditions (probe at the minimum altitude).

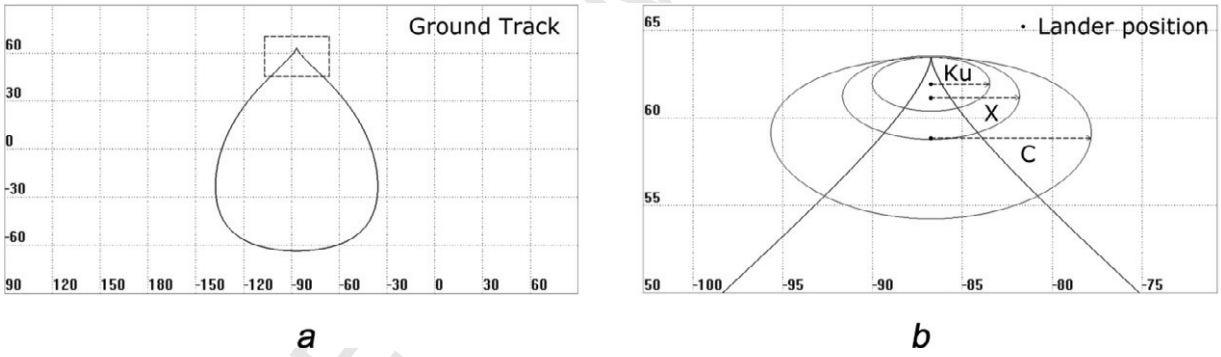

Figure 9. Ground track of solutions A1, optimal lander location and link area in the bands C, X and Ku.

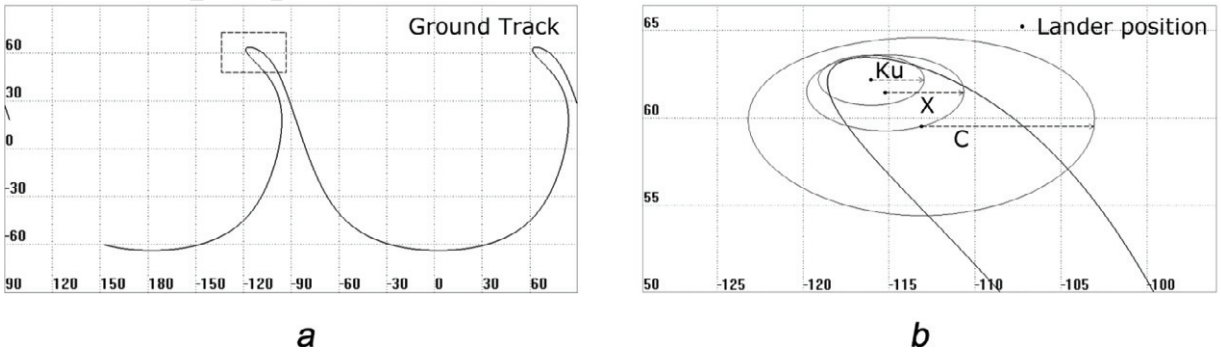

Figure 10. Ground track of solutions B1′, optimal lander location and link area in the bands C, X and Ku.

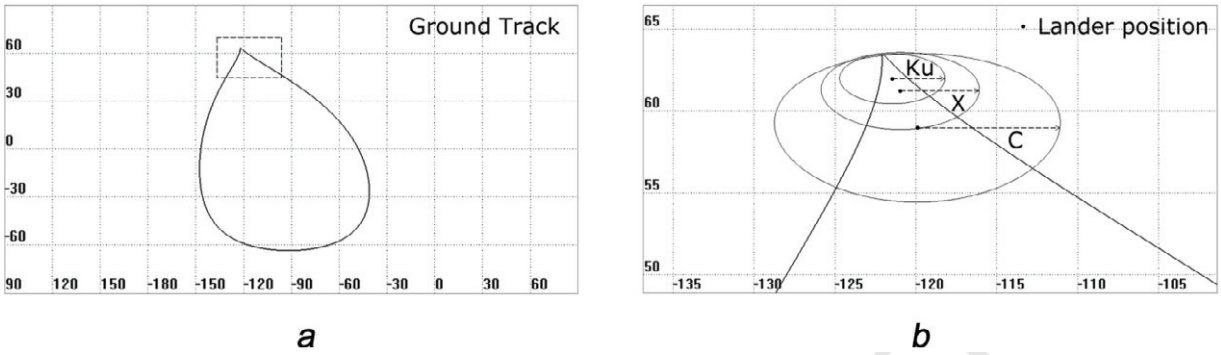

Figure 11. Ground track of solutions A2′, optimal lander location and link area in the bands C, X and Ku.

The link areas, correlated to the angle θ_{3dB} (beam width) in Eq. (15), identifies the loci of probe positions, projected on the surface of the planet, in which the lander-probe contact is possible. In these areas, the sub-probe point presents slow shifts with respect to Mars's surface. According to Eqs. (14) and (15), and keeping the same assumptions introduced in Section 3.4 for the parameters involved in these equations, bands C, X and Ku guarantee, respectively, a maximum gain G of 24.20, 30.22, 33.75 dB and a θ_{3dB} (beam width) of 10.50, 5.25 and 3.50 deg. Thanks to the lower signal frequency, band C provides lower gain but wider link areas. In all the cases, the considered link areas correspond to orbital arcs around the apocentre of the orbits and are therefore located at high latitudes. In fact, the three selected orbits, besides being characterized by a high orbit inclination (63.43 deg), are identified by values of argument of pericentre (270 deg for A1, 255 deg for B1 and A2) which position the apocentre over Mars's high latitudes. The values of the geographical longitude and latitude corresponding to the optimal lander positions are reported in Table 4. Given that the longitudes depend on the RAAN value, which can be chosen according to the area of interest, they have been reported with respect to reference values, corresponding to the longitude of the sub-apocentre points: λ_{A1}, λ_{B1}, λ_{A2} are the longitudes of the sub-apocentre points of solution A1, B1, A2, respectively. The values of λ_{A1}, λ_{B1}, λ_{A2} depend on the RAAN and the epoch.

Optimal lander longitude with respect to the sub-apocentre point [deg]			
Solution	**Band C**	**Band X**	**Band Ku**
A1	λ_{A1}	λ_{A1}	λ_{A1}
B1′	$\lambda_{B1} + 4.50$	$\lambda_{B1} + 2.39$	$\lambda_{B1} + 1.58$
A2′	$\lambda_{A2} - 2.24$	$\lambda_{A2} - 3.30$	$\lambda_{A2} - 3.79$
Optimal lander latitude [deg]			
Solution	**Band C**	**Band X**	**Band Ku**
A1	58.84	61.15	61.92
B1′	59.81	61.44	62.16
A2′	58.97	61.22	61.96

Table 4. Longitudes and latitudes of the optimal lander positions.

Table 5 summarizes the obtained results in terms of daily contact-time, taking into consideration both the non-optimized solutions A1, B1, A2 (Table 2) and the optimal solutions A1′ ≡ A1, B1′, A2′ (Table 3).

Fixed antenna of 0.5 m of diameter			
Synchronous apocentre and lander located at the sub-apocentre point			
Solution	**Contact time in band C [hours: minutes: seconds]**	**Contact time in band X [hours: minutes: seconds]**	**Contact time in band Ku [hours: minutes: seconds]**
A1	4:58:36	3:31:20	2:52:34
B1	3:22:22	1:18:31	0:51:01
A2	5:30:52	1:22:23	0:53:13
Optimal orbit shape and optimal lander position			
Solution	**Contact time in band C [hours: minutes: seconds]**	**Contact time in band X [hours: minutes: seconds]**	**Contact time in band Ku [hours: minutes: seconds]**
A1	6:44:01	4:52:04	4:00:11
B1′	5:00:00	3:09:10	2:08:20
A2′	6:39:37	4:48:24	3:57:05

Table 5. Daily contact times by using a fixed antenna.

For example, for solution A1 in band C the contact time goes from 4 hours and 58 minutes to 6 hours and 44 minutes, presenting an increase of about 35%.

Figs. 12, 13 and 14 show the trends of the azimuth-elevation angles in the link areas, for solutions A1, B1′, A2′, considering the optimal eccentricities and lander positions, in the bands C, X, Ku. All the solutions are characterized by very high elevation angles (always above 84.75 deg).

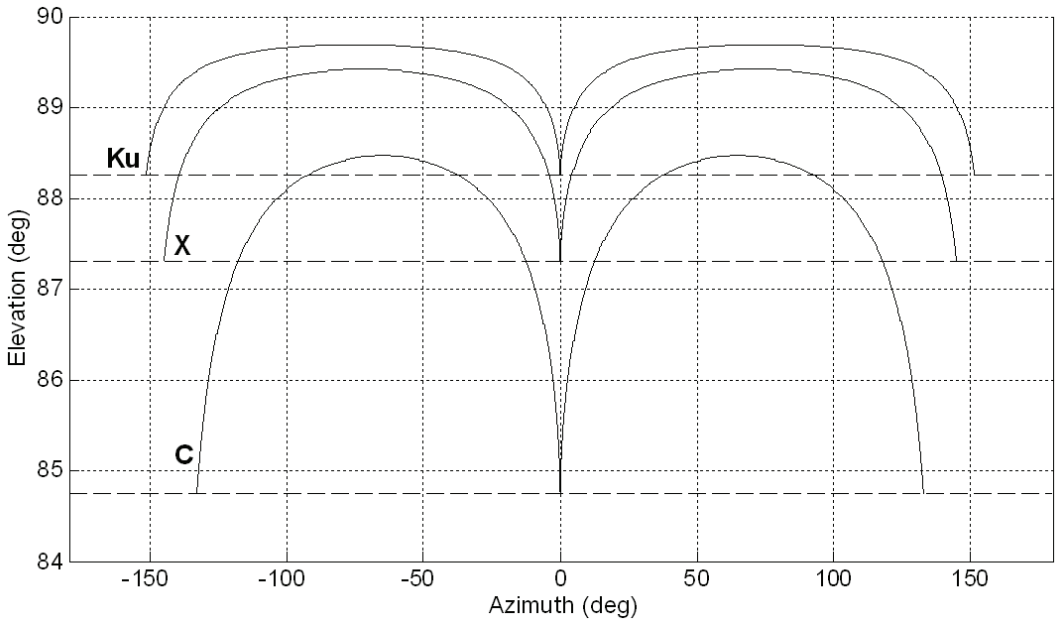

Figure 12. Azimuth-elevation diagrams for solution A1 in bands C, X, Ku.

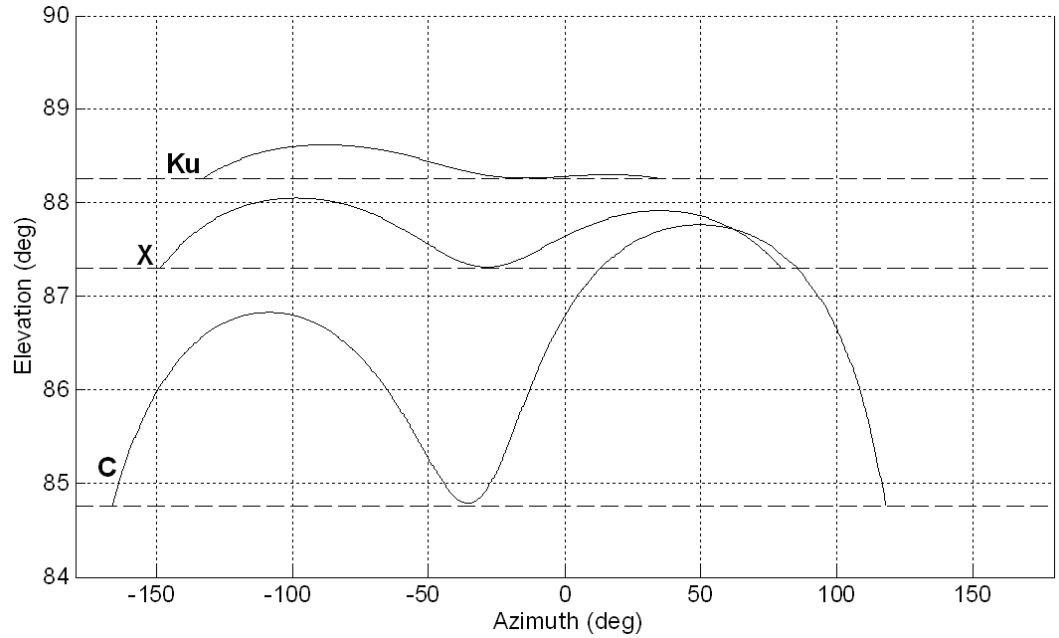

Figure 13. Azimuth-elevation diagrams for solution B1′ in bands C, X, Ku.

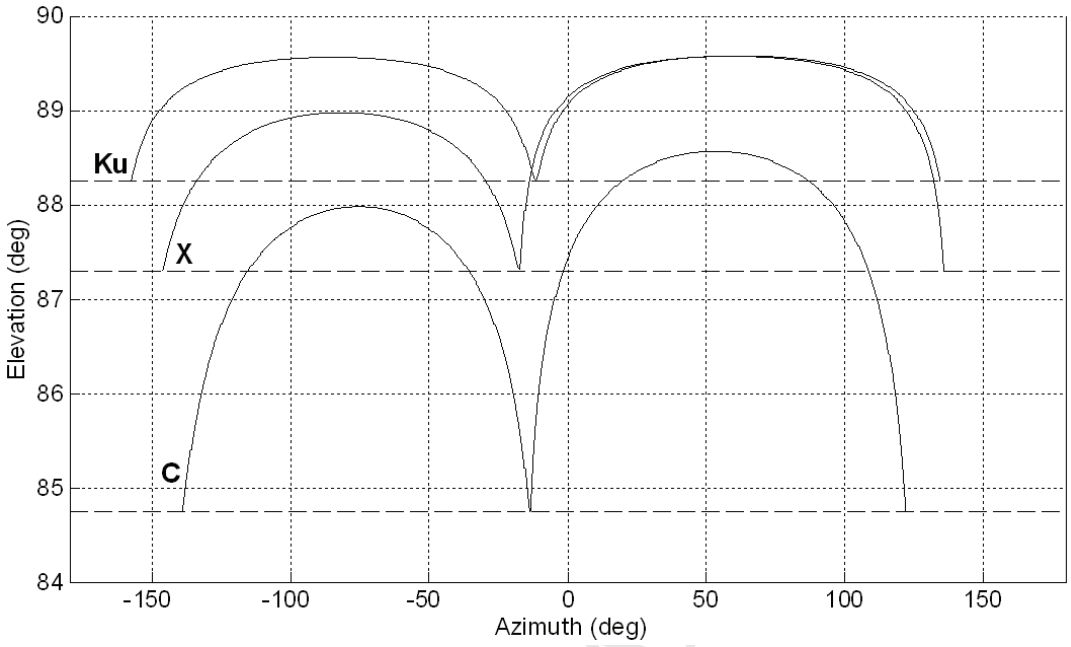

Figure 14. Azimuth-elevation diagrams for solution A2′ in bands C, X, Ku.

In addition, if the antenna installed on board the lander is able to track the probe (mobile antenna), the previous link areas (Figs. 9*b*, 10*b*, 11*b*) enlarge becoming the classical acquisition circles and the contact times increase considerably with respect to ones gained by a fixed antenna: about 19 hours for solutions A1 and A2′, about 18.5 hours for solutions B1′. Figs. 15, 16, 17 show the acquisition circles obtained in the worst conditions (probe at minimum altitude) and considering a minimum elevation angle of 5 deg.

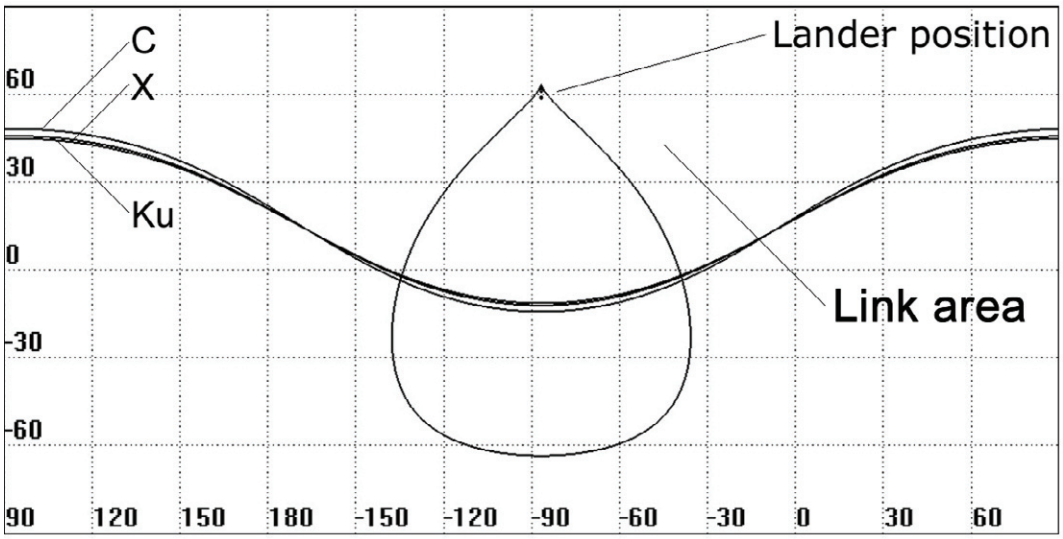

Figure 15. Link area for solution A1.

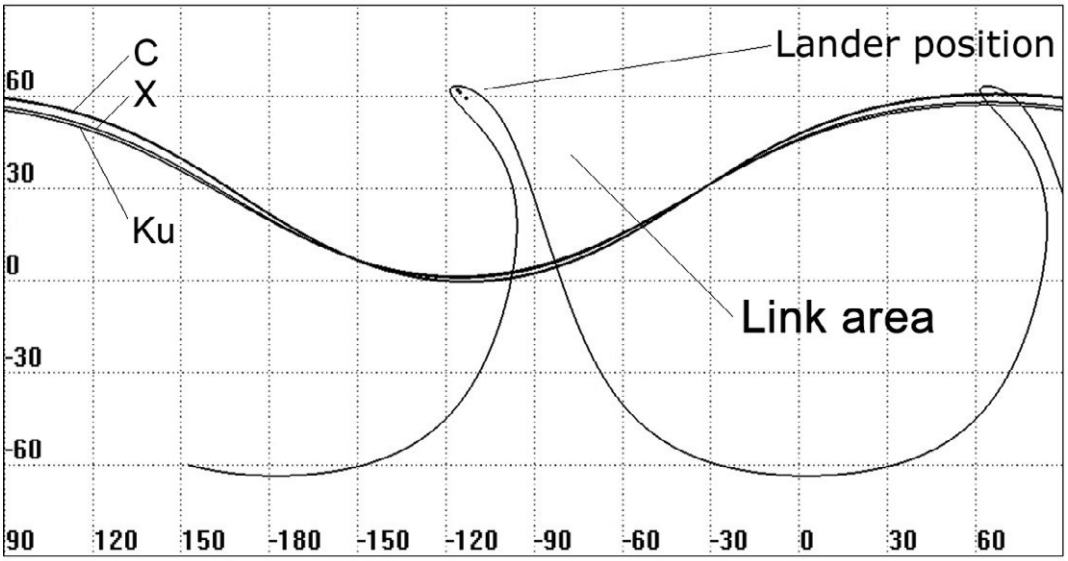

Figure 16. Link area for solution B1′.

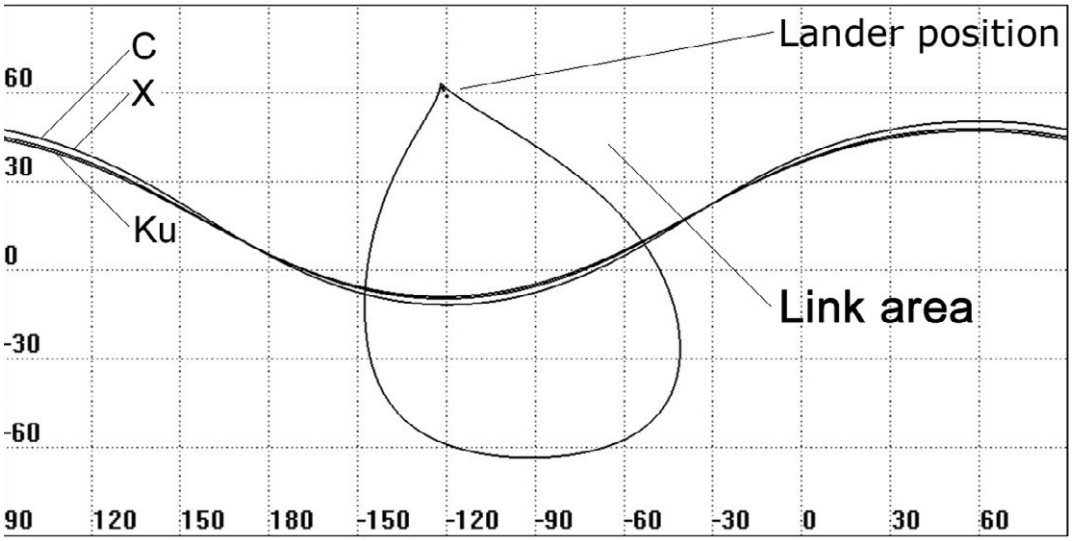

Figure 17. Link area for solution A2′.

In particular, locating appropriately the lander on Mars's equatorial belt, it is feasible to gain a continuous lander-probe link by solution A1 and A2′ (with lower elevation angles). To this purpose, Fig. 18 shows the acquisition circle (in the worst condition) related to solutions A1 in the case of lander positioned on the equator, considering a minimum elevation angle of 5 deg.

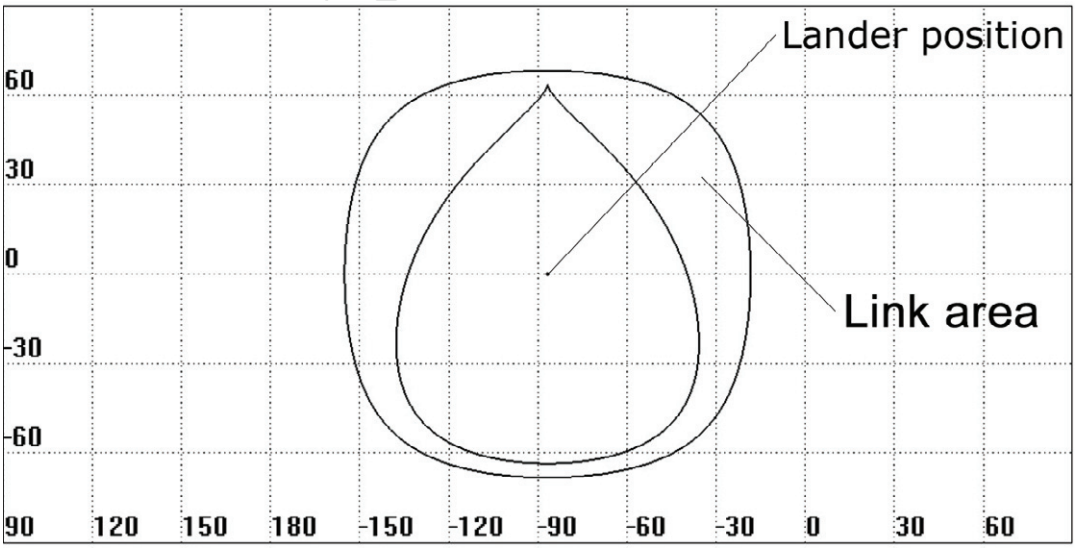

Figure 18. Link area with an equatorial lander for solution A1.

Permanent contact between lander and probe is evident. An analogous condition is gained by solution A2′.

4.1 Analysis of the perturbative effects

As mentioned, Eq. (3) takes into consideration only the planetary oblateness as a perturbative effect. Thus, to investigate the influence of the other gravitational perturbations on the orbit elements of the selected orbits, a numerical analysis has been carried out, considering Mars' gravitational model GMM-2B (Goddard Mars Model 2B) with (80x80) harmonics [15] and the attraction of the Sun. These numerical simulations have highlighted how the only significant differences which are obtained considering the model GMM-2B and the analytical J_2-model are the ones related to the RAAN and to the argument of pericentre. Table 6 reports the annual differences observed ($\Delta\Omega = \Delta\Omega_{(80x80)} - \Delta\Omega_{J2;}\ \Delta\omega = \Delta\omega_{(80x80)} - \Delta\omega_{J2}$, with $\Delta\omega_{J2} = 0$).

Solution	$\Delta\Omega$ [deg/terrestrial year]	$\Delta\omega$ [deg/terrestrial year]
A1	-0.102	1.318
B1′	2.657	2.158
A2′	0.006	-0.334

Table 6. Annual variations due to the higher harmonics of Mars' gravitational field and to the Sun.

While solutions A1 and A2′ keep close to their nominal configurations, solution B1′ is subject to more important variations. In any case, in view of a real mission, a numerical refinement of the orbit elements is always necessary to improve the precision.

5. Conclusions

Orbits at critical inclination allowing long dwell times over a fixed region of Mars and therefore long contact times with a lander located on the surface of the planet have been determined through an investigation into the synchronism conditions between probe and planet. The analysis has led to the selection of three particular solutions, where two are areosynchronous (A1 and A2′) and the other (B1′) is characterized by a nodal period equal to half Mars's nodal day. Different contact times can be gained according to the selected signal frequency. In particular, for the areosynchronous solutions, contact times close to 7 hours per day can be achieved in band C, considering a lander equipped with a fixed antenna having a diameter of 0.5 m and keeping the elevation angle always above 84.75 deg. By a mobile antenna the contact times significantly increase and, if the lander is suitably positioned on Mars's equatorial belt, it is even possible to achieve a continuous link with a probe orbiting in A1 or in A2′.

References

[1] Jai, B., Wenkert, D., Hammer, B., Carlton, M., Johnston, D., Halbrook, T. An Overview of Mars Reconnaissance Orbiter Mission, and Operations Challenges. AIAA SPACE 2007 Conference and Exposition, Long Beach, CA, AIAA Paper 2007-6090, Sept. 2007.

[2] Capderou, M., Forget, F. Optimal orbits for Mars atmosphere remote sensing. Planet. Space Sci. **52**, 789–798, 2004.

[3] Ortore, E., Circi. C., Ulivieri, C., Cinelli, M. Multi-SunSynchronous Orbits in the Solar System. Earth Moon Planets **111(**3-4), 157-172, 2014.

[4] Anderson, P., Macdonald, M. Yen, C., Novel orbits of Mercury, Venus and Mars enabled using low-thrust propulsion. Acta Astronaut. **94**(2), 634-645, 2014.

[5] Liu, X., Baoyin, H., Ma, X. Analytical investigations of quasi-circular frozen orbits in the Martian gravity field. Celest. Mech. Dyn. Astron. **109**, 303–320, 2011.

[6] Lyons, D.T., Beerer, J.G., Esposito, P., Johnston, M.D., Willcockson, W.T. Mars Global Surveyor: Aerobraking Mission Overview. J. Spacecraft Rockets **36**(3), 307–313, 1999.

[7] Golombek, M.P., et al. Overview of the Mars Pathfinder mission: launch through landing, surface operations, data sets, and science results. J. Geophys. Res. **104**(E4), 8523-8553, 1999.

[8] Liu, X., Baoyin, H., Ma, X. Five special types of orbits around Mars. J. Guid. Control Dyn. **33**(4), 1294–1301, 2010.

[9] Liu, X., Baoyin, H., Ma, X. Periodic orbits around areostationary points in the Martian gravity field. Res. Astron. Astrophys. **12**(5), 551–562, 2012.

[10] Silva, J.J., Romero, P. Optimal longitudes determination for the station keeping of areostationary satellites. Planet. Space Sci. **87**, 14-18, 2013.

[11] Alvarellos, J.L. Perturbations on a stationary satellite by the longitude-dependent terms in Mars' gravitational field. J. Astronaut. Sci. **57**(4), 701–715, 2010.

[12] Circi, C., Ortore, E., Bunkheila, F., Ulivieri, C. Elliptical multi-sun-synchronous orbits for Mars exploration. Celest. Mech. Dyn. Astron. **114**(3), 215-227, 2012.

[13] Ortore, E., Circi, C., Bunkheila, F., Ulivieri, C. Earth and Mars observation using periodic orbits. Adv. Space Res. **49**(1), 185-195, 2012.

[14] Maral, G., Bousquet, M. Satellite communications systems, Fourth Edition, Wiley, ISBN: 0471496545, 2003.

[15] Lemoine, F.G., Smith, D.E., Rowlands, D.D., Zuber, M.T., Neumann, G.A., Chinn, D.S. An improved solution of the gravity field of Mars (GMM-2B) from Mars global surveyor. J. Geophys. Res. **106** (E10), 23359–23376, 2001.